Coupling cross-shore and longshore sediment transport to model storm response along a mixed sand-gravel coast under varying wave directions

Rafael J. Bergillos[a,*], Gerd Masselink[b], Miguel Ortega-Sánchez[a]

[a] *Andalusian Institute for Earth System Research, University of Granada, Avda. del Mediterráneo, s/n, 18006, Granada, Spain*
[b] *School of Marine Science and Engineering, Plymouth University, PL4 8AA, Drake Circus, Plymouth, UK*

Abstract

This paper investigates the profile response of a mixed sand-gravel deltaic beach (Playa Granada, southern Spain) forced by storm waves from varying directions. Beach morphology was monitored over a 36-day period with variable wave conditions, and profile response was compared to model predictions using the XBeach-G model and a longshore sediment transport (LST) formulation. XBeach-G was applied over 2-day periods of low energy, south-westerly (SW) storm and south-easterly (SE) storm conditions, and was coupled to LST using a parametric approach which distributes the LST across the swash, surf and nearshore zones. A calibrated wave propagation model (Delft3D) was used to obtain the inshore conditions required to drive the XBeach-G model and the LST formulation. The storm response is clearly influenced by the free-board (difference between the height of the berm and the total run-up) and is also strongly dependent on storm-wave direction, with the SW storm eroding the surveyed area, while the SE storm induced beach accretion. Model results indicate that XBeach-G on its own is capable of adequately reproducing the response of the beach under SW storm conditions (BSS > 0.95), but not under SE

---

[*] Corresponding author.
E-mail address: rbergillos@ugr.es (R.J. Bergillos)

Preprint submitted to Coastal Engineering *July 12, 2017*

storms due to the higher LST gradients at the study location. The combination of XBeach-G and LST fits the measured profiles reasonably well under both SW (BSS > 0.96) and SE (BSS > 0.88) storms, inspiring confidence in the coupled model to predict the storm response under varying wave conditions. The combined XBeach-G/LST model was applied to the entire 6.8-km deltaic coastline to investigate the impact of an extreme SW and SE storm event, and the model results reiterate the importance of cross-shore and longshore sediment transport in driving coastal storm response at this location. The approach proposed in this work can be extended to other worldwide coasts highly influenced by both cross-shore and longshore sediment transport, such as beaches with different coastline orientations and/or forced by varying wave directions.

Keywords: Storm response, beach profile, wave propagation, XBeach-G, longshore sediment transport

---

1. Introduction

Gravel and mixed sand-gravel (MSG) beaches are common in previously para-glaciated coastal regions and coasts with steep hinterlands, and are widespread in the UK (Carter and Orford, 1984; Poate et al., 2016), Denmark (Clemmensen and Nielsen, 2010; Clemmensen et al., 2016), Canada (Engels and Roberts, 2005; Dashtgard et al., 2006), Mediterranean (Bramato et al., 2012; Bergillos et al., 2016c) and New Zealand (Shulmeister and Kirk, 1993; Soons et al., 1997). They are also found when nourishment projects use gravel to protect eroded sandy beaches (López de San Román-Blanco, 2004; Moses and Williams, 2008). Among these coastal settings, a distinction can be made between drift-aligned systems (e.g., Shaw et al. (1990); Carter and Orford (1991)), where alongshore sediment exchange plays the main role in driving shoreline dynamics, and swash-aligned areas (e.g., Orford and Carter (1995); Orford et al. (1995)), which are dominated by cross-shore sediment transport (Forbes et al., 1995; Orford et al., 2002).

Despite their societal importance, the research advances on gravel and MSG beaches are limited compared to those on sandy beaches (Mason et al., 1997; Jennings and Shulmeister, 2002; Pontee et al., 2004; Buscombe and Masselink, 2006; López de San Román-Blanco et al., 2006; Horn and Walton, 2007). This discrepancy is particularly evident for numerical approaches (Orford and Anthony, 2011; Masselink et al., 2014), and contrasts strongly with the increasing demand for reliable coastal change models to help mitigate and adapt to global erosion problems (Syvitski et al., 2005; Anthony et al., 2014) and future sea-level rise (Payo et al., 2016; Spencer et al., 2016). Several efforts have been made over the last decade to develop a morphodynamic storm response model specific to gravel beaches (Pedrozo-Acuña, 2005; Pedrozo-Acuña et al., 2006, 2007; Van Rijn and Sutherland, 2011; Jamal et al., 2011, 2014; Williams et al., 2012). In the present paper, we use the XBeach-G model (McCall et al., 2012, 2013; McCall, 2015), as it has been validated most extensively using both laboratory and field data (McCall et al., 2014, 2015; Almeida et al., 2017).

XBeach-G is a 1D process-based model specifically developed to model cross-shore storm response on gravel beaches. However, in drift-aligned systems, where longshore sediment transport (LST) plays a key role in controlling the coastal behaviour (Orford et al., 1991; López-Ruiz et al., 2014), a cross-shore profile model is clearly not sufficient to model storm response. Drift-aligned systems could be coastlines with a highly variable shoreline orientation and a uni-directional, but spatially-variable LST. Alternatively, they could be coastlines subjected to a bi-directional wave climate characterized by temporal variations in the frequency of the incoming wave directions and, as a consequence, in the net littoral drift (French and Burningham, 2015; Bergillos et al., 2016a). In these coastal areas, it is particularly important to consider not only the cross-shore sediment transport, but also the effects of LST (De Alegría-Arzaburu and Masselink, 2010; Masselink et al., 2016). Recent advances are available to estimate LST on sand, gravel and shingle beaches (Van Rijn, 2014); but the cross-shore distribution of LST, widely studied on sandy beaches (e.g., Berek and Dean (1982); Komar (1983); Kamphuis (1991); Bayram et al. (2001)) and relevant for modelling coastal response, has not been investigated in depth on gravel and MSG beaches (Van Wellen et al., 1998; Van Wellen et al., 2000).

The main objectives of this paper are to characterize and to model the storm response of an MSG beach (Playa Granada, southern Spain) under varying wave directions. Thirteen field surveys were performed and a numerical model (Delft3D) calibrated for the study site was used to relate the wave propagation patterns with the coastal dynamics. Delft3D results were also used to apply and test the XBeach-G model forced by low energy (LE) conditions, and south-westerly (SW) and south-easterly (SE) storms. In addition, XBeach-G was combined with the LST equation of Van Rijn (2014) by means of a parametric formulation to consider different cross-shore distributions of LST. Finally, the approach that best fitted the observed response was used to model extreme SE and SW storms along the entire deltaic coastline, highlighting the potential of the proposed coupled model to extend XBeach-G towards larger longshore scales.

2. Study site

Playa Granada is a 3-km long micro-tidal beach located on the southern coast of Spain that faces the Mediterranean Sea (Figure 1). The beach corresponds to the central stretch of the Guadalfeo deltaic plain (Bergillos et al., 2015c) and is bounded to the west by the Guadalfeo River mouth and to the east by *Punta* *del Santo*, the former location of the river mouth (Figure 1). The deltaic coast is bounded to the west by Salobreña Rock and to the east by Motril Harbour. This harbour is an artificial barrier that prevents LST (Félix et al., 2012).

The Andalusian littoral of the Mediterranean Sea is characterized by the presence of high mountainous relief angles and short fluvial streams. The Guadalfeo River contributes most sediment to the beach (Bergillos et al., 2016d). Its basin covers an area of 1252 km^2, including the highest peaks on the Iberian Peninsula ($\sim$ 3400 m.a.s.l.), and the river is associated with one of the most high-energy drainage systems along the Spanish Mediterranean coast. These steep topographic gradients lead to a wide range of sediment sizes in the Guadalfeo river sediment load (Millares et al., 2014).

Consequently, the particle size distribution on the coast is particularly complex, with varying proportions of sand and gravel. Although three sediment fractions are predominant in the studied coastal area –sand (0.35 mm), fine gravel (5 mm) and coarse gravel (20 mm)– (Bergillos et al., 2015a), the morphodynamic response of the beach is dominated by the coarse gravel fraction due to the selective removal of the finer material (Bergillos et al., 2016c) and the reflective shape of the profile is similar to those found on gravel beaches (Masselink et al., 2010; Poate et al., 2013). Previous numerical works also demonstrated that the best fits to the measured profiles (Bergillos et al., 2016b) and shorelines (Bergillos et al., 2017) are obtained by assuming that the beach is made up of coarse gravel.

The river was dammed 19 km upstream from the mouth in 2004, regulating 85% of the basin run-off (Losada et al., 2011). The total capacity of the Rules' Reservoir (117 hm^3) was planned to be used for the following purposes: irrigation (40%), supplies for residential developments along the coast (19%), energy generation (9%), flood control (30%) and environmental flow (2%). However, as a consequence of river damming, the delta currently experiences coastline retreat and severe erosion problems (Bergillos and Ortega-Sánchez, 2017). The stretch of beach examined, which is occupied by an exclusive hotel complex, golf courses, restaurants and summer homes (Félix et al., 2012), has been particularly affected and has been subjected to higher levels of coastline retreat in recent years than both western and eastern stretches, known as Salobreña and Poniente Beach, respectively (Bergillos et al., 2015b).

Climatic patterns at the study site exhibit a significant contrast between summer and winter. The region is subjected to the passage of extra-tropical Atlantic cyclones and Mediterranean storms with average wind speeds of 18–22 m/s (Ortega-Sánchez et al., 2017) which generate wind waves under fetch-limited conditions (approximately 200 to 300 km). The storm wave climate is bimodal with prevailing W-SW (extra-tropical cyclones) and E-SE (Mediterranean storms) wave directions. The 90%, 99% and 99.9% exceedance significant wave heights in deep water are 1.2 m, 2.1 m and 3.1 m, respectively. The astronomical tidal range is ~ 0.6 m, whereas typical storm surge levels can exceed 0.5 m (Bergillos et al., 2016c).

3. Methodology

3.1. Maritime data and total run-up

A 36-day time series of 864 sea states (hourly hindcasted data for the study period), corresponding to SIMAR point number 2041080 (Figure 1) and provided by *Puertos del Estado*, was used to study the evolution of the following deep-water wave and wind variables: significant wave height (H_0), spectral peak period (T_p), wave direction (θ_0), wind velocity (V_w) and wind direction (θ_w). They were also used as boundary conditions to apply the wave propagation model.

In addition, the total run-up (η) was estimated as the sum of astronomical tide (measured by a gauge located in the Motril Harbour), wind set-up ($\Delta\eta_{\text{wind}}$), barometric set-up ($\Delta\eta_{\text{bar}}$) and wave run-up ($\Delta\eta_{\text{wave}}$). The wind set-up was calculated as $\Delta\eta_{\text{wind}} = \tau_{\text{wind}}/(\rho g h_0)\,\Delta x$ (Bowden, 1983), where g is the acceleration of gravity, $\rho = 1025$ kg/m^3 is the density of salt water, Δx is the wave fetch from the centre of the low-pressure system to the coast (estimated through isobar maps), the depth of the wave base level is represented by $h_0 = L_0/4$, where L_0 is the wavelength in deep water, and the tangential wind stress is obtained from $\tau_{\text{wind}} = \rho_a\, U_*^2$, where ρ_a is the air density and U_* is the friction velocity. The barometric set-up was calculated as $\Delta\eta_{\text{bar}} = \Delta P_a/(\rho g)$ (Dean and Dalrymple, 2002), where ΔP_a represents the atmospheric pressure variation relative to the long-term average pressure at Motril Harbour. The wave run-up was estimated as $\Delta\eta_{\text{wave}} = 0.36\, g^{0.5}\, H_{8,0}^{0.5}\, T_p \tan\beta$ (Nielsen and Hanslow, 1991), where $\tan\beta$ is the intertidal slope and $H_{8,0}$ is the modelled wave height at 8 m water depth de-shoaled to deep water using linear theory and assuming parallel bottom contours. Bergillos et al. (2016c) obtained high correlation (differences less than 9%) between measured and estimated total run-up values with these formulations.

3.2. Field measurements

Thirteen topographic surveys were performed during the 36-day study period (Table 1) to measure the morphology of the beach profile in the central area of the stretch river mouth - *Punta del Santo* (Figure 1). This coastal section is considered representative of the beach behaviour of that section of the coastline (Bergillos et al., 2016c). Each survey was performed under low tide conditions and the observations were referenced to the mean low water spring (MLWS) level.

Topographic measurements were carried out using a highly accurate DGPS

Survey	S1	S2	S3	S4	S5	S6	S7	S8	S9	S10	S11	S12	S13
Date	15/1	16/1	18/1	20/1	22/1	23/1	27/1	30/1	2/2	6/2	9/2	13/2	20/2

Table 1: Timeline of the profile surveys carried out during the study period.

(Javad Maxor) with less than 0.02 m of instrument error. Eleven equally-spaced (10 m) shore-normal profiles were measured (Figure 1) and combined to obtain an alongshore-averaged profile representative of the surveyed area. This alongshore-averaged beach profile was used to address the evolution of the beach under varying wave conditions, as well as for comparison with model predictions.

A high-resolution multibeam bathymetric survey was performed at the beginning of the study period covering the entire deltaic region. Data were acquired using Differential Global Positioning System (DGPS) navigation in reference to the WGS-84 ellipsoid. Accurate navigation and real-time pitch, roll and heave were corrected. A topographic survey along the entire deltaic beach was carried out simultaneously to complement the multibeam bathymetry. These morphological data were used as the bottom boundary conditions for the wave propagation model. To calibrate this model, wave data were continuously collected from December 20th, 2014 to January 30th, 2015 by means of two ADCPs (Figure 1).

3.3. Numerical modelling

3.3.1. Wave propagation model: Delft3D

SIMAR point data for the entire study period (Section 3.1) were propagated from deep-water areas to the nearshore using the WAVE module of the Delft3D model (Lesser et al., 2004; Lesser, 2009), which is based on the SWAN model (Holthuijsen et al., 1993). These results were used to address inshore wave conditions and to provide the boundary conditions for the XBeach-G model and the LST formulation.

The model domain consisted of two different grids, shown in Figure 1. The first is a coarse curvilinear 82x82-cell grid covering the entire deltaic region, with cell sizes that decrease with depth from 170x65 to 80x80 m. The second is a nested grid covering the beach area with 244 and 82 cells in the alongshore and cross-shore directions, respectively, and with cell sizes of approximately 25x15 m. This model was calibrated for the study site by Bergillos et al. (2016a) through comparison with field data, obtaining coefficients of determination equal to 0.86 and 0.89 for the ADCPs A1 and A2 (Figure 1), respectively.

3.3.2. Morphodynamic model of the beach profile: XBeach-G

The 1D process-based model XBeach-G is an extension of the XBeach model that incorporates: (1) a non-hydrostatic pressure correction term that allows solving waves explicitly in model; (2) a groundwater model that allows infiltration and exfiltration; and (3) the computation of bed load transport, including the effects of groundwater ventilation and flow acceleration forces, for estimating bed level changes (McCall et al., 2014, 2015; Masselink et al., 2014).

Bergillos et al. (2016b) has shown that the model is capable of reproducing the morphodynamic response of the beach at the study site under SW storms for a grain size of 20 mm; however, it has not been tested under SE waves. For this reason, XBeach-G was applied to model the profile response of the surveyed area during three 2-day wave windows, depicted in Figure 2, which are representative of LE, SW storm and SE storm conditions. Values of sediment friction factor and Nielsen's boundary layer phase lag used for the simulations were 0.03 and 20°, respectively, which were found to be optimum during the calibration of the model (Bergillos et al., 2016b). These values are slightly different to those found on pure gravel beaches (0.01 and 25°, respectively) by Masselink et al. (2014) and McCall (2015).

Measured topographic data during surveys 6, 7 and 11 were used as initial condition of the upper profile (beach profile above the MLWS level) for the

LE, SW and SE cases, respectively. Measured bathymetric data were used as initial lower profile (beach profile below the MLWS level) for the LE and SW cases since morphological changes between surveys 1 and 7 were comparatively insignificant, whereas the final lower profile for the SW case was used as initial condition for the SE storm. The input wave boundary conditions were obtained from the Delft3D-WAVE model at a depth of 10 m. This water depth offshore boundary fulfils all requirements detailed in the manual of the XBeach-G model (Deltares, 2014), and is deeper than the maximum closure depth in the study site ($\sim$ 9 m according to Bergillos et al. (2016d) and Bergillos et al. (2017)). The infrastructure associated with the hotel complex located landward of the surveyed area (Figure 1) was included in the cross-shore profile as a non-erodible object.

3.3.3. Longshore sediment transport: formulation and cross-shore distribution

To model LST and the ensuing changes in the upper profile, the LST expression proposed by Van Rijn (2014), which was deduced for sand, gravel and shingle beaches, was applied:

$$Q_m = 0.00018\, K_{vr}\, \rho_s\, g^{0.5}\, (\tan\beta)^{0.4}\, D_{50}^{-0.6}\, H_b^{3.1}\, \sin(2\theta_b) \tag{1}$$

where Q_m is the LST rate (dry mass, in kg/s), K_{vr} is a wave correction factor that accounts for the effect of the wave period on the LST rate, $\rho_s = 2650$ kg/m^3 is the sediment density, $\tan\beta$ is the beach slope, D_{50} is the sediment size, H_b is the significant wave height at breaking and θ_b is the wave angle from shore-normal at breaking.

The expression was applied considering alongshore variations in the shoreline, wave variables and beach slope. Surf zone parameters were calculated based on the results of the wave propagation model, obtaining breaking conditions for

69 (shore-normal) beach profiles equally distributed (1 every 100 m) along the coastline between Salobreña Rock and Motril Harbour. The application of this formulation for the coarse gravel fraction ($D_{50} = 20$ mm) was found to provide the best fit to measured morphological changes of the shoreline in the study site (Bergillos et al., 2017). LST gradients were obtained as the ratio between the differences in LST rates among consecutive beach profiles (boundaries) and the distance between them (100 m).

For the cross-shore distribution of the modelled LST volume gradients per meter of shoreline, the following equation was proposed:

$$q = a\,\frac{x}{x_b}\,\exp\left(-k\frac{x}{x_b}\right) \tag{2}$$

where q (in m) is the cross-shore distribution of the LST volume gradient (V, in m^3/m), x is the length across the beach profile ($x = 0$ represents the position of the total run-up), $x_b = s_R + s_b$, where s_R is the length (across the profile) between the total run-up limit and the shoreline, and s_b is the length (across the profile) between the shoreline and the breaking line. The constant k determines where the peak of the cross-shore distribution is located ($k\,x/x_b = 1$), whereas the parameter a (in m) is obtained numerically as a function of V and x_b through the following equation:

$$V = \frac{\partial Q}{\partial l}\Delta t = \int_0^{x_b} q(x)\,dx = \int_0^{x_b} a\,\frac{x}{x_b}\,\exp\left(-k\frac{x}{x_b}\right)dx \tag{3}$$

Through modification of k, this approach can reproduce relatively symmetrical cross-shore distributions of LST reported for sandy beaches (e.g, Bayram et al. (2001)), as well as the asymmetrical distributions on MSG and gravel beaches, whose peaks are expected to be located landward of the peaks on sandy beaches due to the importance of swash processes in gravel environments

(Buscombe and Masselink, 2006). In this work, the profiles resulting from the three values of k were tested, compared and optimised against the observed profile changes ($k_1 = 2$, $k_2 = 5$, $k_3 = 10$).

3.3.4. Coupling XBeach-G and longshore sediment transport

The three 2-day windows of varying wave conditions selected to apply the XBeach-G model (indicated in Figure 2) were also simulated through the combination of XBeach-G and LST. For that, the shape of the final beach profile modelled with XBeach-G was modified after each sea-state considering the LST volume gradients and the three cross-shore distributions of LST detailed in Section 3.3.3.

The goodness of fit for each approach was evaluated through the root-mean-square error (RMSE, in m), the relative bias normalised by the absolute mean of the observations (bias), the correlation coefficient (ρ) and the Brier Skill Score (BSS). All statistics were computed using data interpolated to a regularly-spaced grid and including only points where the measured or modelled bed level changes were greater than the maximum between the estimated instrument error and $3D_{50}$, according to McCall et al. (2015). Following the criteria proposed by Van Rijn et al. (2003), the fits were qualified from *bad* to *excellent* based on the BSS values.

Finally, the impact of extreme SW and SE storms ($H_{99.9\%}$) was modelled using both XBeach-G and the coupled model for the entire 6.8-km deltaic coastline to further determine the importance of cross-shore and longshore sediment transport in driving storm response under varying wave directions. The modelled wave variables were $H_0 = 3.1$ m, $T_p = 8.4$ s (the most frequent period under storm conditions), $\theta_{0,\mathrm{SW}} = 238°$ and $\theta_{0,\mathrm{SE}} = 107°$ (the most frequent directions under SW and SE storms, respectively). These sea states, summarized in Table 2, were simulated considering a storm surge (η_{ss}) of 0.5 m for two different durations: 6 hours around high tide and 12 hours representing a full tidal cycle.

	SW storm	SE storm
H_0 (m)	3.1	3.1
T_p (s)	8.4	8.4
θ_0 (°)	238	107
η_{ss}	0.5	0.5

Table 2: Sea-states modelled with XBeach-G and XBeach-G/LST to study storm response under varying wave directions along the entire deltaic coastline.

4. Results

4.1. Wave, wind and water level conditions

The deep-water significant wave height and the spectral peak period were lower than 1 m and 6 s during the 56.3% and 62% of the study period, respectively (Figure 2a-b). These values are significantly lower than average percentages from January 1958 till the end of the study period (84.6% and 83.8%, respectively, based on the SIMAR 2041080 data), indicating that the beach was forced by relatively high energy waves during this 36-day period. The predominant deep-water wave directions were $180° < \theta_0 < 270°$ (SW sector, 50.9% of the time) and $90° < \theta_0 < 180°$ (SE sector, 36% of the time). This period was, thus, more westerly-dominated than the average (41.6% and 55.7%, respectively), in agreement with the trend in wave direction over last six years (Bergillos et al., 2016a). The average wind velocity was 7.4 m/s, with prevailing values less than 10 m/s (73.3% of the time) and incoming directions from the W-SW and E-SE (Figure 2d).

Two extreme storms ($H_0 > H_{99.9\%}$) occurred with maximum H_0 of 4.9 m and 3.2 m, and maximum T_p equal to 9.2 s and 8.4 s, respectively. The first storm, which occurred between surveys 7 and 9 (S7-S9), was associated with westerly waves ($\theta_0 \in [235°, 239°]$); whereas the second storm, during period S11-S12, was forced by easterly waves ($\theta_0 \in [104°, 117°]$). The maximum V_w during storms

1 and 2 were 19.9 m/s and 16.5 m/s with θ_w from the W-SW (extra-tropical Atlantic cyclone) and the E-SE (Mediterranean storm), respectively. The SW storm was the second most severe since 1958. The maximum total run-up (sum of the astronomical tide, storm surge and wave run-up) during this storm was 2.6 m (Figure 2e), generating overwash along the entire beach profile (Section 4.3).

4.2. Wave propagation patterns in the nearshore zone

Figure 3 depicts the spatial distribution of the time-averaged energy flux (in W/m) between surveys 1-7, 7-10 and 10-13 according to Delft3D-WAVE modelling. Nearshore wave energy levels were comparatively insignificant during S1-S7 (Figure 3a), when the average wave height ($H_0 = 0.62$ m), mean period ($T_z = 2.95$ s) and peak period ($T_p = 4.19$ s) were the lowest, and the percentages of SW-SE waves were the most balanced (46.9%-30.5%). Between S7 and S10, the highest values of nearshore wave energy were concentrated in the studied section of coastline due to the prevailing SW waves during this period (Figure 2c).

Nearshore wave energy levels between S10 and S13 were significantly lower than those over the period S7-S10 (Figure 3b-c). Considering that the average values of mean and peak wave periods were similar ($T_z = 4.13$ s and $T_p = 6.01$ s during S7-S10 *vs* $T_z = 4.15$ s and $T_p = 6.26$ during S10-S13), the lower energy levels over S10-S13 are attributable to both the less average wave height ($H_0 = 1.54$ m *vs* $H_0 = 1.34$ m) and the more balanced percentages of SW-SE waves (75.8%-4.6% *vs* 36.7%-63.1%). The dominance of SE waves during S10-S13 generated higher energy levels along the section *Punta del Santo* - Motril Harbour compared to those in Playa Granada (Figure 3c). This highlights the importance of the incoming wave directions in the nearshore wave propagation patterns, with direct implications in the profile response.

4.3. Observed morphological response of the upper profile

Three different profile responses were observed during the study period (Figure 4). The morphological changes were relatively insignificant between S1 and S7 due to the lower total run-up and energy level over this period (Figures 2e and 3a), but the profile strongly eroded during S7-S9 induced by the extreme SW storm. The profile could not be completely measured during S8 since it coincided with the beginning of the overwash (Figure 5a); therefore, the morphology of this profile at elevations below 1.5 m should be taken with caution (Figure 4b). Beach recovery occurred between S10 and S13 influenced by the medium energy content during this period (Figures 3c and 4c). This is in agreement with observations of Bramato et al. (2012) on a nearby MSG beach, who found that a minimum wave energy is required not only to erode the beach, but also to recover it. It is suggested, and demonstrated in Section 4.5, that the SE storm between S11 and S12 contributed to this recovery due to LST.

Figure 6 depicts the maximum total run-up, the minimum free-board (difference between the height of the berm and the maximum total run-up) and the volumetric changes above the MLWS level (in m^3 per unit m of shoreline, or m^2) between surveys. It is observed how between S1 and S7, dominated by swash regime, accretion rates were lower than 0.36 m^2/day; whereas between S7 and S9, when overwash occurred, the average erosion rate was 2.56 m^2/day. Beach recovery up to 1.1 m^2/day took place between S9 and S13, with positive values of the free-board over this whole period. The destruction of the berms between S7 and S9 and the subsequent generation of new berm deposits are also observed in the lower panel of Figure 6, which shows the cross-shore distribution of the bed level changes between surveys. These patterns confirm the importance of the overwash process (Matias et al., 2014) and the total run-up (Bergillos et al., 2016c) dictating beach response.

4.4. Modelling profile response with XBeach-G

Figure 7 shows the initial, final measured and final modelled profiles with XBeach-G, along with the differences in the cross-shore distance measured (ΔX_{Meas}) and predicted (ΔX_{Mod}) for the three temporal windows indicated in Figure 2. As expected, the XBeach-G model does not reproduce the relatively small ($\Delta X_{\text{Meas}} < 0.5$ m) accretional changes observed under LE conditions; however, the fit between modelled and measured bed level variations forced by the SW storm is *excellent* (BSS = 0.96), with RMSE < 0.14 m and bias < 0.13 (Table 3). This indicates that the model is capable of reproducing the response of the studied coastline section under SW storm conditions, which is in agreement with previous results of the model for two less energetic SW storms in December 2013 and March 2014 (Bergillos et al., 2016b).

The comparison of pre- and post-storm measured profiles under SE waves reveals that accretion took place across the upper profile. This deposition was mainly concentrated at an elevation of $1.2-1.3$ m, coinciding with the total run-up during this window (Figure 2e) and contrasting with the erosion predicted by the model at this location (Figure 7c). This behaviour is influenced by the higher LST gradients for SE storms with respect to those for SW conditions (Section 4.5), and highlights the need to combine the XBeach-G results with LST gradients to provide more confident predictions of the morphological response under SE storm conditions.

	Low energy conditions				South-westerly storm				South-easterly storm			
	RMSE	bias	ρ	BSS	RMSE	bias	ρ	BSS	RMSE	bias	ρ	BSS
XBeach-G	0.02	-0.73	0.117	0.007	0.134	0.125	0.966	0.956	0.175	-1.122	0.564	0.137
LST (k=2)	0.015	-0.076	0.519	0.453	0.103	0.091	0.967	0.962	0.082	-0.503	0.91	0.768
LST (k=5)	0.014	-0.068	0.523	0.457	0.09	0.072	0.966	0.964	0.057	-0.269	0.938	0.887
LST (k=10)	0.015	0.074	0.521	0.455	0.092	-0.11	0.961	0.963	0.099	0.516	0.929	0.662

Table 3: Root-mean-square error (RMSE, in m), relative bias (bias), correlation coefficient (ρ) and Brier Skill Score (BSS) of the modelled changes relative to the measurements of the upper profile.

4.5. Modelling profile response with XBeach-G and longshore sediment transport

To couple XBeach-G and longshore processes, LST rates along the entire deltaic coastline were computed for the three 2-day windows on the basis of the formulation of Van Rijn (2014), detailed in Section 3.3.3. The results indicate that the time-averaged LST rates during the SW storm were greater in the section *Punta del Santo* - Motril Harbour (up to 0.038 m^3/s) than in the studied section (up to 0.02 m^3/s). However, the opposite occurred over the SE storm, except in the vicinity of Motril Harbour, where the shoreline alignment is NW-SE, inducing higher breaking angles from shore-normal (Figure 8). The maximum and time-averaged LST rates (in absolute value) along the section Guadalfeo River mouth - *Punta del Santo* during the SE storm were up to 0.025 m^3/s (90 m^3/h) and 0.013 m^3/s (46.8 m^3/h), respectively. These values were similar to those under the SW storm (0.022 m^3/s and 0.02 m^3/s, respectively), which was a significantly more energetic window ($H_{\mathrm{max,SW}} = 4.9$ m and $H_{\mathrm{mean,SW}} = 3.2$ m *vs* $H_{\mathrm{max,SE}} = 3.2$ m and $H_{\mathrm{mean,SE}} = 2.1$ m), revealing the importance of LST in this coastal section forced by SE conditions. The average LST rates over the LE window were two orders of magnitude lower than those obtained for both storms (Figure 8).

Figure 9 details the LST rates during the entire study period for the surveyed area, whose boundaries are indicated in Figures 1 and 8. It is observed that the difference in breaking angles and LST rates between the two boundaries was greater under SE wave conditions, inducing higher gradients in the LST rates and volumes. In addition, the breaking depths and cross-shore distances were significantly lower over the SE storm window than those during the SW window, i.e., LST was concentrated in a smaller width across the nearshore zone, resulting in higher bed level changes across the upper beach profile for the SE storm. To model this cross-shore distribution of LST volume, three different options were tested based on the parametric approach reported in Section 3.3.3.

The cross-shore distributions for each sea state of the three modelled windows are shown in Figure 10. The LST distribution for $k = 2$ is the most uniform with the maximum located in the middle between the total run-up limit and the breaking line (at $x/x_b = 0.5$). This distribution is similar to that previously observed on sandy beaches (Berek and Dean, 1982; Bayram et al., 2001). The LST distribution for $k = 10$ is the most asymmetrical with the maximum located at $x/x_b = 0.1$, concentrating most of the LST in the inner nearshore region (Figure 10a3-d3). This behaviour is considered more typical of gravel beaches, where the surf zone does not exist and most of the sediment transport occurs in the swash zone (Buscombe and Masselink, 2006). The LST distribution for $k = 5$ is intermediate between the previous two, with the maximum located at $x/x_b = 0.2$, which is suggested to be expected for MSG beaches. These three cross-shore distributions were used to combine XBeach-G and LST, updating the morphology of the beach profile after each sea state by means of the computed total run-up locations, breaking lengths across the profile and LST volume gradients (Figure 9).

The results of the coupling for the three simulated windows and the three tested cross-shore distributions are shown in Figure 11. The goodness-of-fit parameters obtained for the different model approaches are summarized in Table 3. The best model performance (lower RMSE-bias and higher ρ-BSS) is obtained for the combination of XBeach-G and LST considering the intermediate cross-shore distribution of LST ($k = 5$, Figure 10a2-d2), with the only exception of the slightly higher ρ with $k = 2$ for the SW storm (Table 3). The intermediate approach improves the XBeach-G results for LE easterly conditions, although the fit for this case is only *fair* (BSS = 0.46). However, the obtained fits for both SW and SE storms are *excellent* (BSS = 0.96 and BSS = 0.89, respectively), inspiring confidence in the proposed approach to model the storm response under varying wave conditions. The improvements with respect to the XBeach-G results are primarily relevant under SE storms ($|\Delta\text{RMSE}| > 0.11$ m, $|\Delta\text{bias}| > 0.85$, $\Delta\rho > 0.37$ and $\Delta\text{BSS} > 0.7$). These results reveal the importance of LST on the coastal response of the surveyed area under SE wave conditions.

4.6. Storm response along the coastline under varying wave directions

Figure 12 depicts the volumetric changes of the upper profile along the entire 6.8-km deltaic coastline modelled with XBeach-G and through the combination of XBeach-G and LST for $k = 5$. It is observed how XBeach-G predicts beach erosion along most of the coastline, with only some relatively low depositional changes in the stretch Salobreña Rock - *Punta del Santo* (western section) and *Punta del Santo* - Motril Harbour (eastern section) for SE and SW storms, respectively. As expected, volumetric changes on the basis of the XBeach-G results are significantly higher along the western (eastern) section under SW (SE) storms (Figure 12b1-b2).

Results with the coupled model for SW storm conditions show more erosion than those obtained with XBeach-G along most of the western section, and also show accretion rather than erosion along most of the eastern section (Figure 12b1-c1). Under SE storms, the combined approach reverts XBeach-G results along the section Guadalfeo River mouth - *Punta del Santo* (Figure 12b2-c2), predicting depositional rather than erosional changes, and in agreement with the observations reported in Section 4.3. Results along the eastern section reveal larger erosion than XBeach-G predictions in the vicinity of *Punta del Santo* and accretion instead of erosion near Motril Harbour, influenced by the LST patterns at these locations under SE storms. The variations between both models for such conditions are significantly lower in the stretch Salobreña Rock - Guadalfeo River mouth due to the less LST gradients along this section under SE waves

(Figure 8).

The comparison between the two simulated periods indicates that most of the morphological changes are induced by cross-shore and longshore sediment transport during high tide. During low tide conditions, beach recovery takes place at some locations of the western (eastern) section under SW (SE) storms (Figure 12), highlighting the importance of the total run-up and overwash process dictating beach response. The results of this section show the potential of the coupled approach proposed in this work to provide more confident predictions of the storm response on coasts dominated by both cross-shore and longshore sediment transport.

5. Conclusions

Although gravel and MSG coasts have received increasing attention during recent years, relatively few numerical models have been applied to and compared with field data for these coastal settings. This paper studies and models the storm response of Playa Granada (southern Spain) under varying wave directions by means of field measurements, the application of the XBeach-G model and the proposal of a parametric approach to couple XBeach-G and LST. Based on the observations and results, the following conclusions were drawn:

1. The morphological storm response is clearly related to the difference between the height of the berm and the total run-up (i.e., the free-board). Wave propagation patterns are influenced by the incoming wave directions, generating varying values of total run-up and resulting in different beach responses, with the SW and SE storms eroding and building up the surveyed area, respectively.
2. The XBeach-G model is capable of reproducing the storm response of the beach under SW waves, with BSS > 0.95 and a relative bias < 0.13.

However, the accretionary response of the upper profile under SE storms contrasts with the erosion predicted by the model (BSS < 0.14 and $|\text{bias}| > 1.12$). This is influenced by the higher LST gradients under SE storms at the study location compared to those under SW conditions, revealing the necessity to combine XBeach-G with LST.

3. The coupling of XBeach-G and the LST equation of Van Rijn (2014), through consideration of different cross-shore distributions of LST, improved the model predictions, especially under SE storm conditions. The best fits (BSS > 0.96 and BSS > 0.88 for the SW and SE storms, respectively) were obtained with a distribution where the peak of the LST volume is located at a distance from the total run-up limit equal to 20% of the length across the profile between this limit and the breaking line, providing insights into the cross-shore distribution of LST on MSG beaches.
4. The approach that best fitted the beach response was applied to model extreme SW and SE storms along a 6.8-km section of deltaic coastline. Erosional changes were obtained along most of the western section for the SW storm, and in the eastern section and to the west of the river mouth for the SE storm. Erosion occurred in particular under high tide conditions. In contrast, the coupled model predicted accretion along most of the eastern section and in the stretch river mouth - *Punta del Santo* under SW and SE storms, respectively. These depositional responses were not predicted by the XBeach-G model on its own. Thus, the approach proposed in this paper represents an extension of XBeach-G to make it more suitable for gravel and MSG coasts highly influenced by both cross-shore and longshore sediment transport.

Acknowledgements

This research was supported by the project CTM2012-32439 (Secretaría de Estado de I+D+i, Spain) and the research group TEP-209 (Junta de Andalucía). Rafael J. Bergillos was funded by the Ministry of Economy and Competitiveness (Spain) through Research Contract BES-2013-062617 and Mobility Grants EEBB-I-15-10002 and EEBB-I-16-11009. Gerd Masselink was funded by EPSRC grant EP/H040056/1 and NERC grant NE/N015525/1. We would like to thank Robert T. McCall and Miguel A. Losada for their helpful advice. We also acknowledge two anonymous reviewers for their improvements to this paper.

References

Almeida, L.P., Masselink, G., McCall, R., Russell, P., 2017. Storm overwash of a gravel barrier: Field measurements and XBeach-G modelling. Coastal Engineering 120, 22–35.

Anthony, E.J., Marriner, N., Morhange, C., 2014. Human influence and the changing geomorphology of Mediterranean deltas and coasts over the last 6000 years: From progradation to destruction phase? Earth-Science Reviews 139, 336–361.

Bayram, A., Larson, M., Miller, H.C., Kraus, N.C., 2001. Cross-shore distribution of longshore sediment transport: comparison between predictive formulas and field measurements. Coastal Engineering 44, 79–99.

Berek, E.P., Dean, R.G., 1982. Field investigation of longshore transport distribution, in: Coastal Engineering Proceedings, 1(18).

Bergillos, R.J., López-Ruiz, A., Ortega-Sánchez, M., Masselink, G., Losada, M.A., 2016a. Implications of delta retreat on wave propagation and longshore sediment transport - Guadalfeo case study (southern Spain). Marine Geology 382, 1–16.

Bergillos, R.J., Masselink, G., McCall, R.T., Ortega-Sánchez, M., 2016b. Modelling overwash vulnerability along mixed sand-gravel coasts with XBeach-G: Case study of Playa Granada, southern Spain, in: Coastal Engineering Proceedings.

Bergillos, R.J., Ortega-Sánchez, M., 2017. Assessing and mitigating the landscape effects of river damming on the Guadalfeo River delta, southern Spain. Landscape and Urban Planning 165, 117–129.

Bergillos, R.J., Ortega-Sánchez, M., Losada, M.A., 2015a. Foreshore evolution of a mixed sand and gravel beach: The case of Playa Granada (Southern Spain), in: Proceedings of the 8th Coastal Sediments, World Scientific.

Bergillos, R.J., Ortega-Sánchez, M., Masselink, G., Losada, M.A., 2015b. Urban planning analysis of Mediterranean deltas - Guadalfeo case study, in: 12th International Conference on the Mediterranean Coastal Environment, pp. 143–154.

Bergillos, R.J., Ortega-Sánchez, M., Masselink, G., Losada, M.A., 2016c. Morpho-sedimentary dynamics of a micro-tidal mixed sand and gravel beach, Playa Granada, southern Spain. Marine Geology 379, 28–38.

Bergillos, R.J., Rodríguez-Delgado, C., López-Ruiz, A., Millares, A., Ortega-Sánchez, M., Losada, M.A., 2015c. Recent human-induced coastal changes in the Guadalfeo river deltaic system (southern Spain), in: Proceedings of the 36th IAHR-International Association for Hydro-Environment Engineering and Research World Congress: http://89.31.100.18/~iahrpapers/87178.pdf.

Bergillos, R.J., Rodríguez-Delgado, C., Millares, A., Ortega-Sánchez, M., Losada, M.A., 2016d. Impact of river regulation on a Mediterranean delta: assessment of managed versus unmanaged scenarios. Water Resources Research 52, 5132–5148.

Bergillos, R.J., Rodríguez-Delgado, C., Ortega-Sánchez, M., 2017. Advances in management tools for modeling artificial nourishments in mixed beaches. Journal of Marine Systems, 172, 1–13.

Bowden, K.F., 1983. Physical oceanography of coastal waters. Ellis Horwood Ltd., Chichester England.

Bramato, S., Ortega-Sánchez, M., Mans, C., Losada, M.A., 2012. Natural recovery of a mixed sand and gravel beach after a sequence of a short duration storm and moderate sea states. Journal of Coastal Research 28, 89–101.

Buscombe, D., Masselink, G., 2006. Concepts in gravel beach dynamics. Earth-Science Reviews 79, 33–52.

Carter, R.W.G., Orford, J.D., 1984. Coarse clastic barrier beaches: a discussion of the distinctive dynamic and morphosedimentary characteristics. Developments in Sedimentology 39, 377–389.

Carter, R.W.G., Orford, J.D., 1991. The sedimentary organisation and behaviour of drift-aligned gravel barriers, in: Proceedings of the 3rd Coastal Sediments, ASCE. pp. 934–948.

Clemmensen, L.B., Glad, A.C., Kroon, A., 2016. Storm flood impacts along the shores of micro-tidal inland seas: A morphological and sedimentological study of the Vesterlyng beach, the Belt Sea, Denmark. Geomorphology 253, 251–261.

Clemmensen, L.B., Nielsen, L., 2010. Internal architecture of a raised beach ridge system (Anholt, Denmark) resolved by ground-penetrating radar investigations. Sedimentary Geology 223, 281–290.

Dashtgard, S.E., Gingras, M.K., Butler, K.E., 2006. Sedimentology and stratigraphy of a transgressive, muddy gravel beach: Waterside Beach, Bay of Fundy, Canada. Sedimentology 53, 279–296.

De Alegría-Arzaburu, A.R., Masselink, G., 2010. Storm response and beach rotation on a gravel beach, Slapton Sands, UK. Marine Geology 278, 77–99.

Dean, R.G., Dalrymple, R.A., 2002. Coastal processes with engineering applications. Cambridge University Press, New York.

Deltares, 2014. XBeach-G GUI 1.0. User Manual. Delft, The Netherlands.

Engels, S., Roberts, M.C., 2005. The architecture of prograding sandy-gravel beach ridges formed during the last Holocene highstand: Southwestern British Columbia, Canada. Journal of Sedimentary Research 75, 1052–1064.

Félix, A., Baquerizo, A., Santiago, J.M., Losada, M.A., 2012. Coastal zone management with stochastic multi-criteria analysis. Journal of Environmental Management 112, 252–266.

Forbes, D.L., Orford, J.D., Carter, R.W.G., Shaw, J., Jennings, S.C., 1995. Morphodynamic evolution, self-organisation, and instability of coarse-clastic barriers on paraglacial coasts. Marine Geology 126, 63–85.

French, J., Burningham, H., 2015. Wave-driven sediment pathways on a gravel-dominated coast subject to a strongly bi-modal wave climate, Suffolk, eastern UK, in: Proceedings of the 8th Coastal Sediments, World Scientific.

Holthuijsen, L., Booij, N., Ris, R., 1993. A spectral wave model for the coastal zone, in: Ocean Wave Measurement and Analysis, ASCE. pp. 630–641.

Horn, D.P., Walton, S.M., 2007. Spatial and temporal variations of sediment size on a mixed sand and gravel beach. Sedimentary Geology 202, 509–528.

Jamal, M.H., Simmonds, D.J., Magar, V., 2014. Modelling gravel beach dynamics with XBeach. Coastal Engineering 89, 20–29.

Jamal, M.H., Simmonds, D.J., Magar, V., Pan, S., 2011. Modelling infiltration on gravel beaches with an XBeach variant, in: Coastal Engineering Proceedings, 1(32).

Jennings, R., Shulmeister, J., 2002. A field based classification scheme for gravel beaches. Marine Geology 186, 211–228.

Kamphuis, J., 1991. Alongshore sediment transport rate distribution, in: Proceedings of the 3rd Coastal Sediments, ASCE. pp. 170–183.

Komar, P.D., 1983. Nearshore currents and sand transport on beaches. Elsevier oceanography series 35, 67–109.

Lesser, G.R., 2009. An approach to medium-term coastal morphological modeling. Ph.D. thesis. Department of Civil Engineering, Delft University of Technology, Delft, The Netherlands.

Lesser, G.R., Roelvink, J.A., Van Kester, J.A.T.M., Stelling, G.S., 2004. Development and validation of a three-dimensional morphological model. Coastal Engineering 51, 883–915.

López de San Román-Blanco, B., 2004. Dynamics of gravel and mixed sand and gravel beaches. Ph.D. thesis. Imperial College, London, UK.

López de San Román-Blanco, B., Coates, T.T., Holmes, P., Chadwick, A.J., Bradbury, A., Baldock, T.E., Pedrozo-Acuña, A., Lawrence, J., Grüne, J., 2006. Large scale experiments on gravel and mixed beaches: Experimental procedure, data documentation and initial results. Coastal Engineering 53, 349–362.

López-Ruiz, A., Ortega-Sánchez, M., Baquerizo, A., Losada, M.A., 2014. A note on alongshore sediment transport on weakly curvilinear coasts and its implications. Coastal Engineering 88, 143–153.

Losada, M.A., Baquerizo, A., Ortega-Sánchez, M., Ávila, A., 2011. Coastal evolution, sea level, and assessment of intrinsic uncertainty. Journal of Coastal Research , 218–228.

Mason, T., Voulgaris, G., Simmonds, D.J., Collins, M.B., 1997. Hydrodynamics and sediment transport on composite (Mixed Sand/Shingle) and sand beaches: a comparison, in: Proceedings of the 3rd Coastal Dynamics, ASCE. pp. 48–57.

Masselink, G., McCall, R.T., Poate, T., Van Geer, P., 2014. Modelling storm response on gravel beaches using XBeach-G, in: Proceedings of the Institution of Civil Engineers-Maritime Engineering, Thomas Telford Ltd. pp. 173–191.

Masselink, G., Russell, P., Blenkinsopp, C., Turner, I.L., 2010. Swash zone sediment transport, step dynamics and morphological response on a gravel beach. Marine Geology 274, 50–68.

Masselink, G., Scott, T., Poate, T., Russell, P., Davidson, M., Conley, D., 2016. The extreme 2013/2014 winter storms: hydrodynamic forcing and coastal response along the southwest coast of England. Earth Surface Processes and Landforms 41, 378–391.

Matias, A., Blenkinsopp, C.E., Masselink, G., 2014. Detailed investigation of overwash on a gravel barrier. Marine Geology 350, 27–38.

McCall, R.T., 2015. Process-based modelling of storm impacts on gravel coasts. Ph.D. thesis. Plymouth University, UK.

McCall, R.T., Masselink, G., Poate, T., Bradbury, A., Russell, P., Davidson, M., 2013. Predicting overwash on gravel barriers. Journal of Coastal Research 65, 1473–1478.

McCall, R.T., Masselink, G., Poate, T.G., Roelvink, J.A., Almeida, L.P., 2015. Modelling the morphodynamics of gravel beaches during storms with XBeach-G. Coastal Engineering 103, 52–66.

McCall, R.T., Masselink, G., Poate, T.G., Roelvink, J.A., Almeida, L.P., Davidson, M., Russell, P.E., 2014. Modelling storm hydrodynamics on gravel beaches with XBeach-G. Coastal Engineering 91, 231–250.

McCall, R.T., Masselink, G., Roelvink, D., Russell, P., Davidson, M., Poate, T., 2012. Modelling overwash and infiltration on gravel barriers, in: Coastal Engineering Proceedings, 1(33).

Millares, A., Polo, M.J., Moñino, A., Herrero, J., Losada, M.A., 2014. Bedload dynamics and associated snowmelt influence in mountainous and semiarid alluvial rivers. Geomorphology 206, 330–342.

Moses, C.A., Williams, R.B.G., 2008. Artificial beach recharge: the South East England experience. Zeitschrift für Geomorphologie, Supplementary Issues 52, 107–124.

Nielsen, P., Hanslow, D.J., 1991. Wave runup distributions on natural beaches. Journal of Coastal Research 7, 1139–1152.

Orford, J.D., Anthony, E.J., 2011. Extreme events and the morphodynamics of gravel-dominated coastal barriers: Strengthening uncertain ground. Marine Geology 290, 41–45.

Orford, J.D., Carter, R.W.G., 1995. Examination of mesoscale forcing of a swash-aligned, gravel barrier from Nova Scotia. Marine Geology 126, 201–211.

Orford, J.D., Carter, R.W.G., Jennings, S.C., 1991. Coarse clastic barrier environments: evolution and implications for Quaternary sea level interpretation. Quaternary International 9, 87–104.

Orford, J.D., Carter, R.W.G., McKenna, J., Jennings, S.C., 1995. The relationship between the rate of mesoscale sea-level rise and the rate of retreat of swash-aligned gravel-dominated barriers. Marine Geology 124, 177–186.

Orford, J.D., Forbes, D.L., Jennings, S.C., 2002. Organisational controls, typologies and time scales of paraglacial gravel-dominated coastal systems. Geomorphology 48, 51–85.

Ortega-Sánchez, M., Bergillos, R.J., López-Ruiz, A., Losada, M.A., 2017. Morphodynamics of Mediterranean Mixed Sand and Gravel Coasts. Springer.

Payo, A., Mukhopadhyay, A., Hazra, S., Ghosh, T., Ghosh, S., Brown, S., Nicholls, R.J., Bricheno, L., Wolf, J., Kay, S., Lázár, A.N., Haque, A., 2016. Projected changes in area of the Sundarban mangrove forest in Bangladesh due to SLR by 2100. Climatic Change, 1–13.

Pedrozo-Acuña, A., 2005. Concerning swash on steep beaches. Ph.D. thesis. University of Plymouth, UK.

Pedrozo-Acuña, A., Simmonds, D.J., Chadwick, A.J., Silva, R., 2007. A numerical–empirical approach for evaluating morphodynamic processes on gravel and mixed sand–gravel beaches. Marine Geology 241, 1–18.

Pedrozo-Acuña, A., Simmonds, D.J., Otta, A.K., Chadwick, A.J., 2006. On the cross-shore profile change of gravel beaches. Coastal Engineering 53, 335–347.

Poate, T., Masselink, G., Davidson, M., McCall, R.T., Russell, P., Turner, I., 2013. High frequency in-situ field measurements of morphological response on a fine gravel beach during energetic wave conditions. Marine Geology 342, 1–13.

Poate, T.G., McCall, R.T., Masselink, G., 2016. A new parameterisation for runup on gravel beaches. Coastal Engineering 117, 176–190.

Pontee, N.I., Pye, K., Blott, S.J., 2004. Morphodynamic behaviour and sedimentary variation of mixed sand and gravel beaches, Suffolk, UK. Journal of Coastal Research 20, 256–276.

Shaw, J., Taylor, R.B., Forbes, D.L., 1990. Coarse clastic barriers in eastern Canada: patterns of glaciogenic sediment dispersal with rising sea levels. Journal of Coastal Research 9, 160–200.

Shulmeister, J., Kirk, R.M., 1993. Evolution of a mixed sand and gravel barrier system in North Canterbury, New Zealand, during Holocene sea-level rise and still-stand. Sedimentary Geology 87, 215–235.

Soons, J.M., Shulmeister, J., Holt, S., 1997. The Holocene evolution of a well nourished gravelly barrier and lagoon complex, Kaitorete Spit, Canterbury, New Zealand. Marine Geology 138, 69–90.

Spencer, T., Schuerch, M., Nicholls, R.J., Hinkel, J., Lincke, D., Vafeidis, A.T., Reef, R., McFadden, L., Brown, S., 2016. Global coastal wetland change under sea-level rise and related stresses: the diva wetland change model. Global and Planetary Change 139, 15–30.

Syvitski, J.P.M., Vörösmarty, C.J., Kettner, A.J., Green, P., 2005. Impact of humans on the flux of terrestrial sediment to the global coastal ocean. Science 308, 376–380.

Van Rijn, L., Walstra, D., Grasmeijer, B., Sutherland, J., Pan, S., Sierra, J., 2003. The predictability of cross-shore bed evolution of sandy beaches at the time scale of storms and seasons using process-based profile models. Coastal Engineering 47, 295–327.

Van Rijn, L.C., 2014. A simple general expression for longshore transport of sand, gravel and shingle. Coastal Engineering 90, 23–39.

Van Rijn, L.C., Sutherland, J.R., 2011. Erosion of gravel barriers and beaches, in: Proceedings of the 7th Coastal Sediments, World Scientific.

Van Wellen, E., Chadwick, A.J., Mason, T., 2000. A review and assessment of longshore sediment transport equations for coarse-grained beaches. Coastal Engineering 40, 243–275.

Van Wellen, E., Shadwick, A.J., Lee, M., Baily, B., Morfett, J., 1998. Evaluation of longshore sediment transport models on coarse grained beaches using field data: A preliminary investigation, in: Coastal Engineering Proceedings, 1(26).

Williams, J.J., de Alegría-Arzaburu, A.R., McCall, R.T., Van Dongeren, A., 2012. Modelling gravel barrier profile response to combined waves and tides using XBeach: Laboratory and field results. Coastal Engineering 63, 62–80.

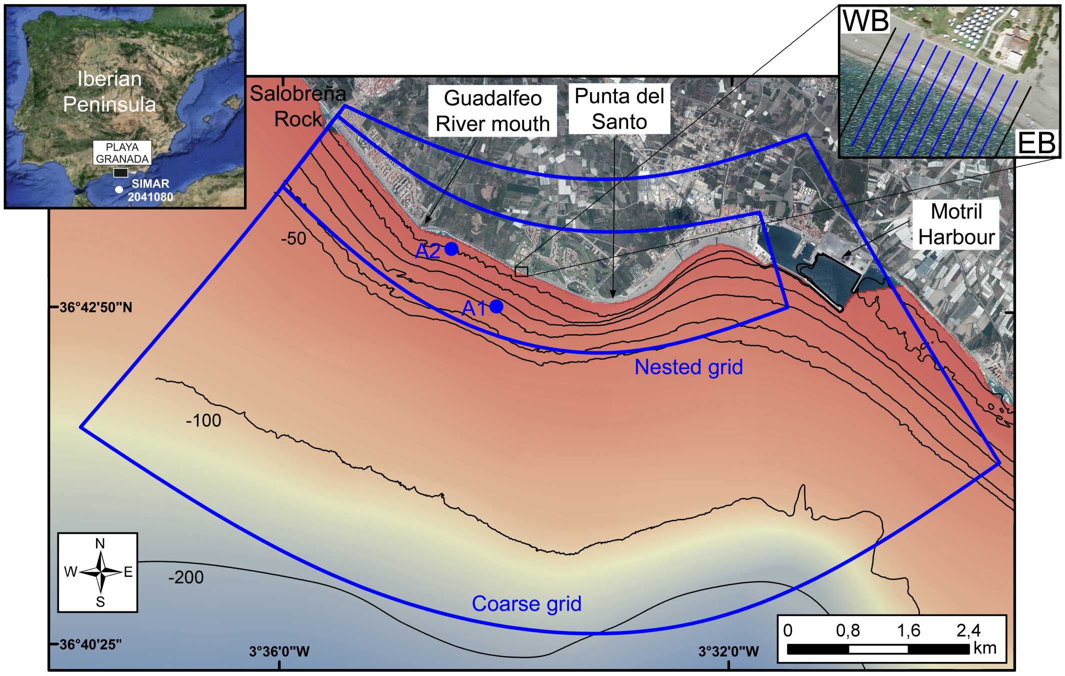

Figure 1: Upper left panel: Location of the study site (Playa Granada, southern Spain) and the SIMAR point 2041080. Central panel: bathymetric contours, grids used in the wave propagation model and positioning of the ADCPs (A1 and A2). Upper right panel: west (WB) and east (EB) boundaries of the surveyed area and measured beach profiles.

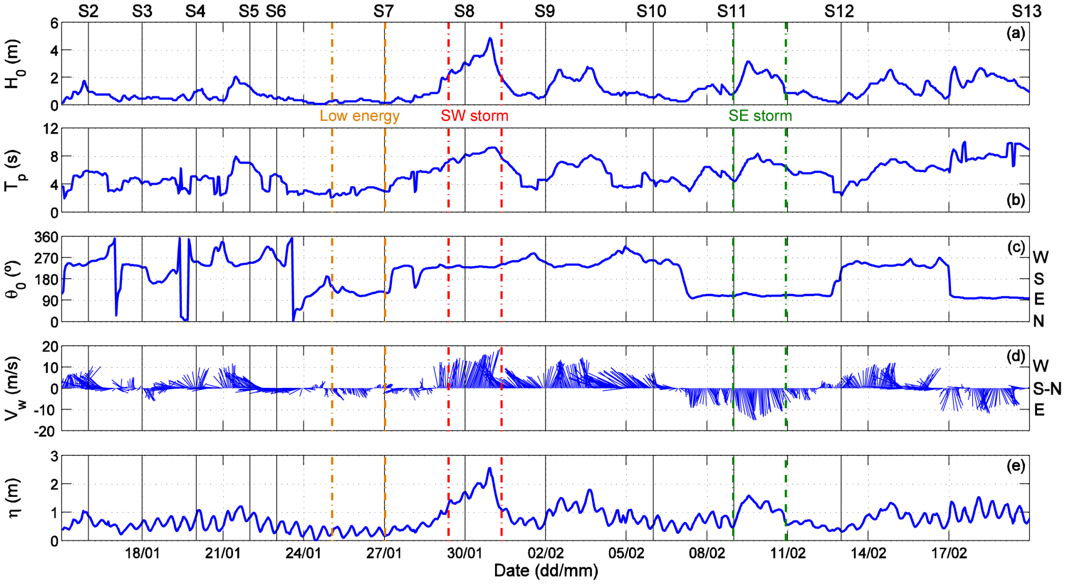

Figure 2: Evolution of the deep-water significant wave height (a), spectral peak period (b), wave direction (c), wind velocity and direction (d), and total run-up (e) over the study period. The vertical black lines indicate the date of the field surveys and the vertical coloured lines delimitate the windows selected to model the profile response.

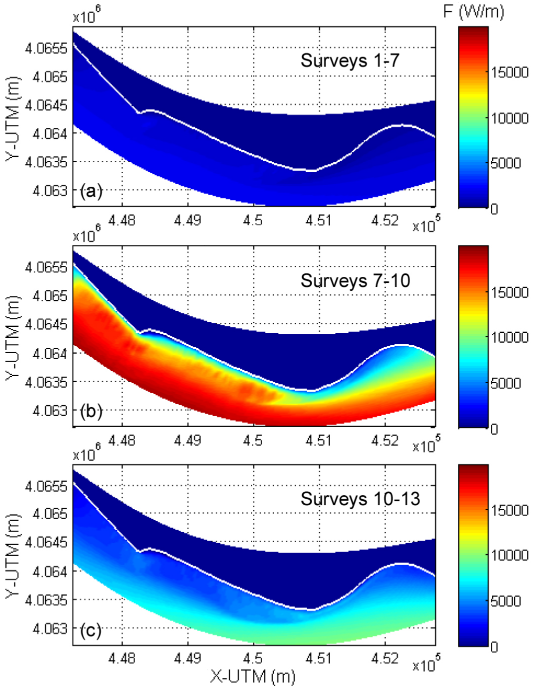

Figure 3: Spatial distribution of the time-averaged energy flux (in W/m) modelled with Delft3D-WAVE: (a) surveys 1-7 (low energy conditions), (b) surveys 7-10 (south-westerly storm), and (c) surveys 10-13 (south-easterly storm). The shorelines are highlighted in white.

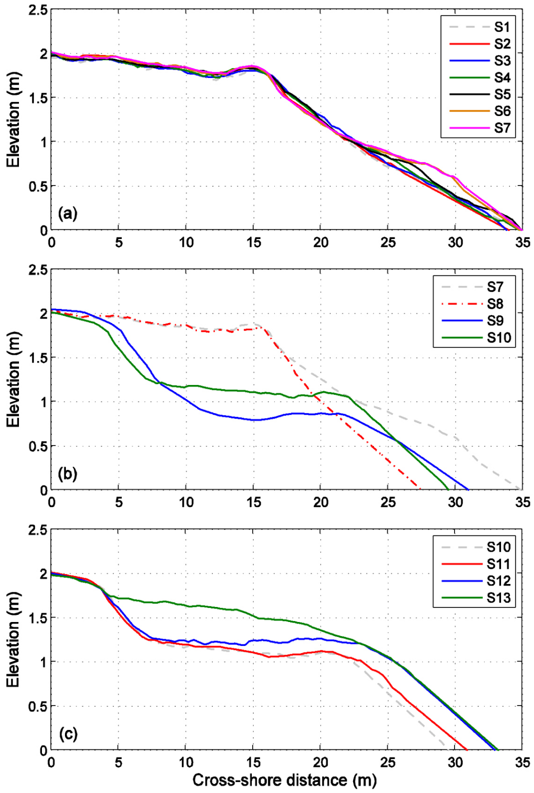

Figure 4: Evolution of the upper profile during the study period: (a) surveys 1-7 (low energy conditions), (b) surveys 7-10 (south-westerly storm), and (c) surveys 10-13 (south-easterly storm). Elevation = 0 indicates the MLWS level.

Figure 5: (a) Beginning of the overwash process during the south-westerly storm (survey 8). (b) Beginning of the south-easterly storm (survey 11).

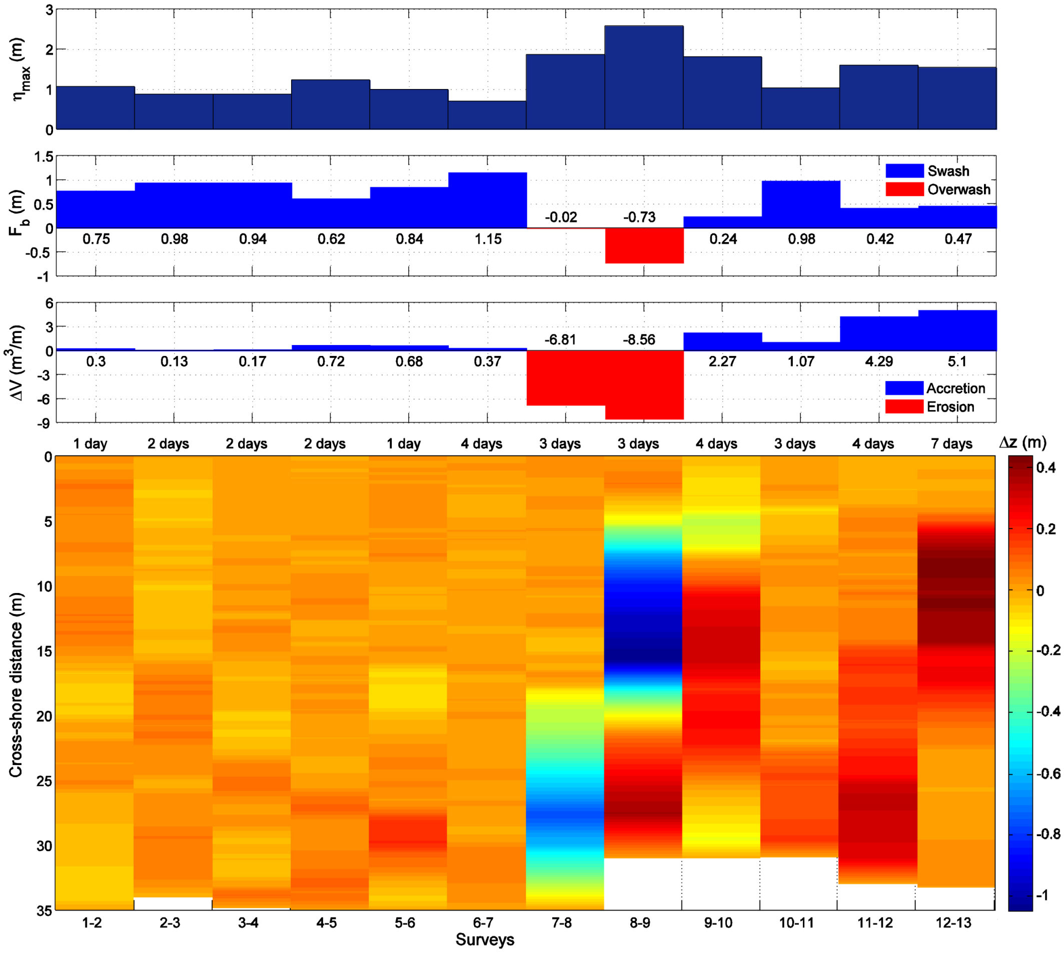

Figure 6: From top to bottom: maximum total run-up before each survey, minimum freeboard before each survey, unit volume differences above the MLWS level between surveys, and bed level changes above the MLWS level between surveys. The number of days between surveys is indicated in the lower panel. The white colour in the lower panel is due to coastline retreat.

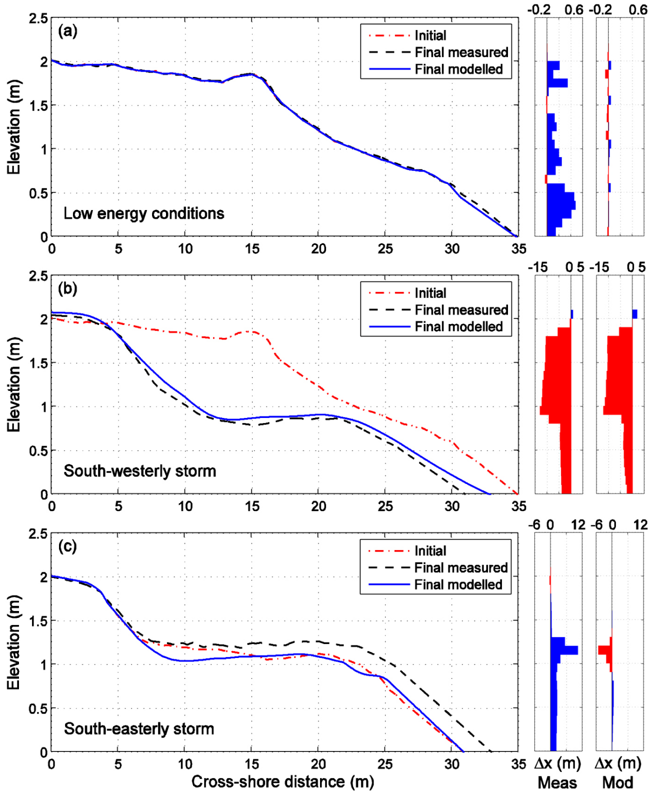

Figure 7: Initial, final measured and final modelled profiles with XBeach-G: (a) low energy conditions window, (b) south-westerly storm, and (c) south-easterly storm. Elevation = 0 indicates the MLWS level. Differences in measured (Meas) and modelled (Mod) cross-shore distances between profiles (Δx) are indicated in the right panels.

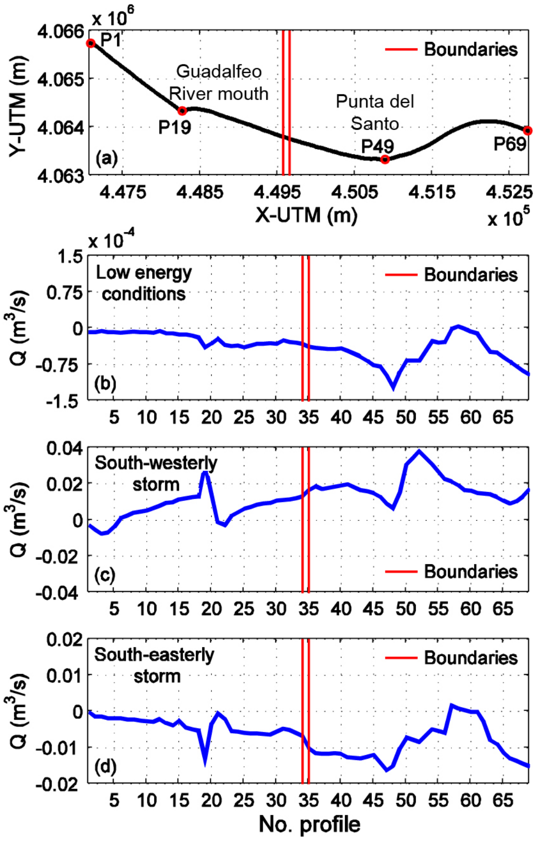

Figure 8: Alongshore evolution of the time-averaged LST rates: (b) low energy conditions window, (c) south-westerly storm, and (d) south-easterly storm. The shoreline and four profile locations are shown in panel a.

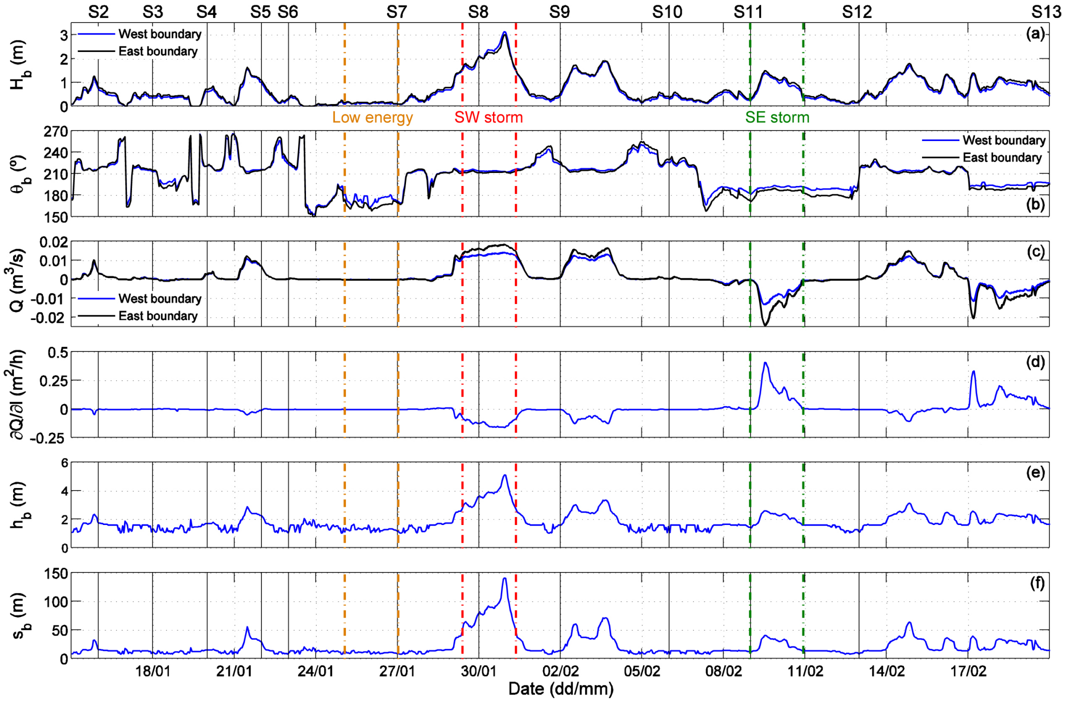

Figure 9: Evolution of the breaking wave height (a), breaking wave direction (b), LST rate (c), LST gradient (d), breaking depth (e), and breaking cross-shore distance (f) during the study period. The vertical black lines indicate the date of the field surveys and the vertical coloured lines delimitate the windows selected to model the profile response.

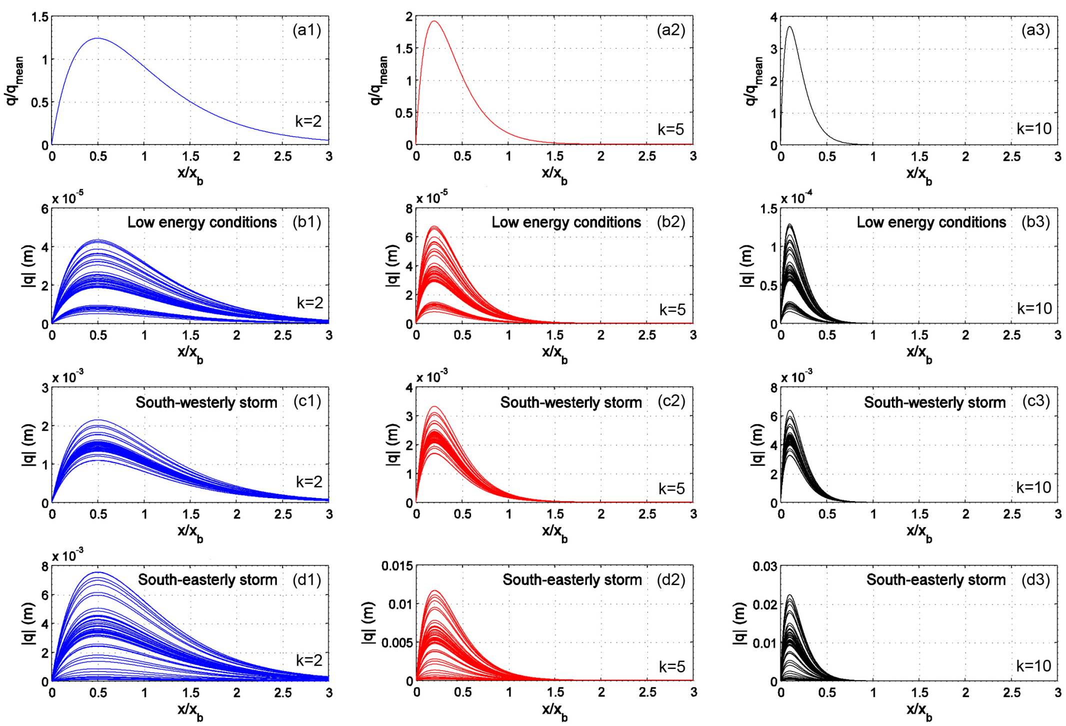

Figure 10: Normalized cross-shore distribution of LST for $k = 2$ (a1), $k = 5$ (a2), and $k = 10$ (a3). Cross-shore distribution during the low energy conditions window (b), the south-westerly storm (c), and the south-easterly storm (d) for k=2 (1), k=5 (2), and k=10 (3).

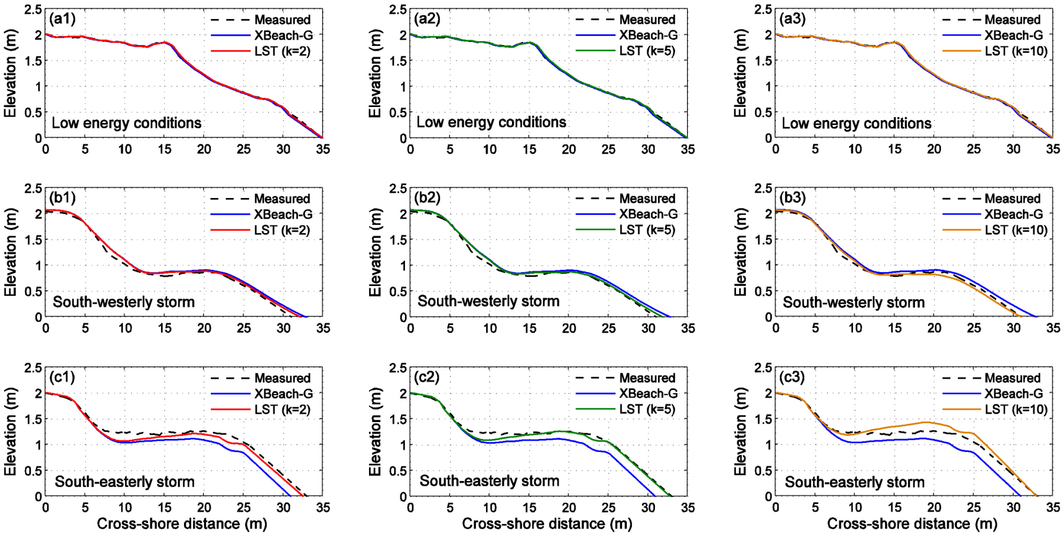

Figure 11: Initial, final measured and final modelled profiles with XBeach-G and LST: (a) low energy conditions window, (b) south-westerly storm, and (c) south-easterly storm for $k = 2$ (1), $k = 5$ (2), and $k = 10$ (3). Elevation = 0 indicates the MLWS level.

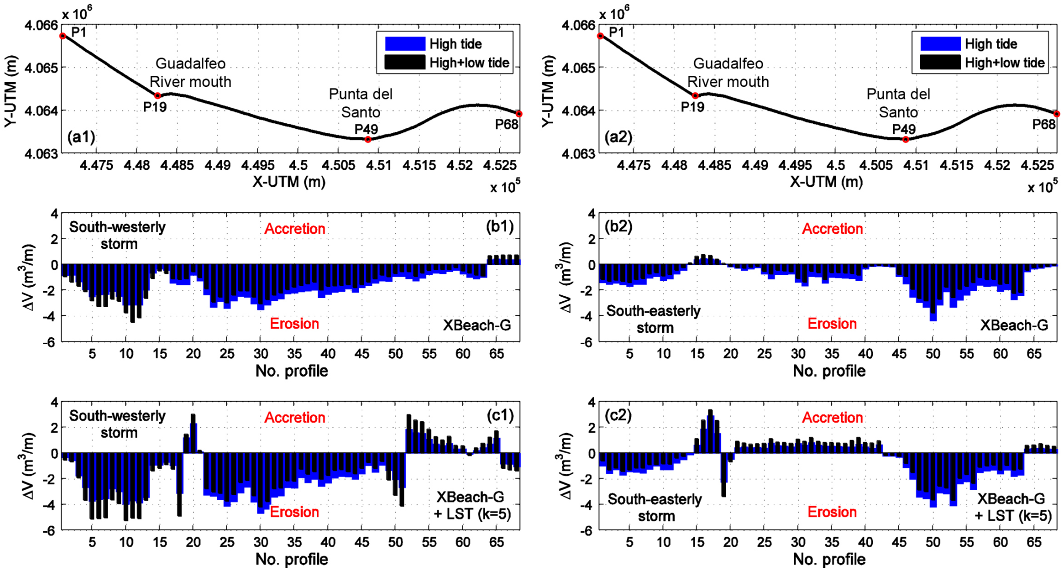

Figure 12: Alongshore evolution of the modelled volumetric changes on the beach (above the MLWS level) with XBeach-G (b) and coupling XBeach and LST (c) for south-westerly (1) and south-easterly (2) storm conditions. The shoreline and four profile locations are shown in panels a1 and a2.